Myosteatosis: diagnostic significance and assessment by imaging approaches

Ana Isabel Garcia-Diez[1,2,3,4]^, Marta Porta-Vilaro[1]^, Jaime Isern-Kebschull[1]^, Natali Naude[5]^, Roman Guggenberger[6]^, Laura Brugnara[3,4]^, Ana Milinkovic[7]^, Alvaro Bartolome-Solanas[1]^, Juan Carlos Soler-Perromat[1]^, Montserrat Del Amo[1,2], Anna Novials[3,4]^, Xavier Tomas[1]^

[1]Department of Radiology, Hospital Clínic de Barcelona, Barcelona, Spain; [2]Faculty of Medicine, Universitat de Barcelona, Barcelona, Spain; [3]August Pi i Sunyer Biomedical Research Institute (IDIBAPS), Hospital Clínic de Barcelona, Barcelona, Spain; [4]Spanish Biomedical Research Centre in Diabetes and Associated Metabolic Disorders (CIBERDEM), Madrid, Spain; [5]Institute of Glycomics, Griffith University, Gold Coast, Queensland, Australia; [6]Institute of Diagnostic and Interventional Radiology, University Hospital Zurich, Switzerland; [7]Chelsea and Westminster Foundation NHS Hospital Trust, Imperial College London, London, UK

Contributions: (I) Conception and design: AI Garcia-Diez, M Porta-Villaro, J Isern-Kebschull, L Brugnara, A Milinkovic; (II) Administrative support: M Del Amo, A Novials, X Tomas; (III) Provision of study materials or patients: AI Garcia-Diez, N Naude, R Guggenberger, A Milinkovic; (IV) Collection and assembly of data: J Isern-Kebschull, A Bartolome-Solanas, JC Soler-Perromat; (V) Data analysis and interpretation: AI Garcia-Diez, M Porta-Villaro, L Brugnara; (VI) Manuscript writing: All authors; (VII) Final approval of manuscript: All authors.

Correspondence to: Ana Isabel Garcia-Diez, MD, PhD. Department of Radiology, Hospital Clínic de Barcelona, Villarroel 170, 08036 Barcelona, Spain; Faculty of Medicine, Universitat de Barcelona, Barcelona, Spain; August Pi i Sunyer Biomedical Research Institute (IDIBAPS), Hospital Clínic de Barcelona, Barcelona, Spain; Spanish Biomedical Research Centre in Diabetes and Associated Metabolic Disorders (CIBERDEM), Madrid, Spain. Email: aigarcia@clinic.cat.

Abstract: Myosteatosis has emerged as an important concept in muscle health as it is associated with an increased risk of adverse health outcomes, a higher rate of complications, and increased mortality associated with ageing, chronic systemic and neuromuscular diseases, cancer, metabolic syndromes, degenerative events, and trauma. Myosteatosis involves ectopic infiltration of fat into skeletal muscle, and it exhibits a negative correlation with muscle mass, strength, and mobility representing a contributing factor to decreased muscle quality. While myosteatosis serves as an additional biomarker for sarcopenia, cachexia, and metabolic syndromes, it is not synonymous with sarcopenia. Myosteatosis induces proinflammatory changes that contribute to decreased muscle function, compromise mitochondrial function, and increase inflammatory response in muscles. Imaging techniques such as computed tomography (CT), particularly opportunistic abdominal CT scans, and magnetic resonance imaging (MRI) or magnetic resonance spectroscopy (MRS), have been used in both clinical practice and research. And in recent years, ultrasound has emerged as a promising bedside tool for measuring changes in muscle tissue. Various techniques, including CT-based muscle attenuation (MA) and intermuscular adipose tissue (IMAT) quantification, MRI-based proton density fat fraction (PDFF) and T1–T2 mapping, and musculoskeletal ultrasound (MSUS)-based echo intensity (EI) and shear wave elastography (SWE), are accessible in clinical practice and can be used as adjunct biomarkers of myosteatosis to assess various debilitating muscle health conditions. However, a stan¬dard definition of myosteatosis with a thorough understanding of the pathophysiological mechanisms, and a consensus in assessment methods and clinical outcomes has not yet been established. Recent developments in

^ ORCID: Ana Isabel Garcia-Diez, 0000-0002-8573-6628; Marta Porta-Villaro, 0000-0002-7462-5586; Jaime Isern-Kebschull, 0000-0001-6789-000X; Natali Naude, 0000-0002-4941-4285; Roman Guggenberger, 0000-0002-5903-2248; Laura Brugnara, 0000-0002-9896-5024; Ana Milinkovic, 0000-0002-7732-9168; Alvaro Bartolome-Solanas, 0000-0002-2307-0007; Juan Carlos Soler-Perromat, 0000-0002-2552-3903; Anna Novials, 0000-0003-0465-2949; Xavier Tomas, 0000-0003-2189-8721.

image acquisition and quantification have attempted to develop an appropriate muscle quality index for the assessment of myosteatosis. Additionally, emerging studies on artificial intelligence (AI) may provide further insights into quantification and automated assessment, including MRS analysis. In this review, we discuss the pathophysiological aspects of myosteatosis, all the current imaging techniques and recent advances in imaging assessment as potential biomarkers of myosteatosis, and the most common clinical conditions involved.

Introduction

Quantitative evaluation of muscle characteristics is of increasing interest in musculoskeletal research and clinical practice. The rise in life expectancy has resulted in a progressive increase in the prevalence of degenerative, metabolic, and chronic diseases. Muscle changes associated with age, inactivity, malnutrition, chronic systemic and neuromuscular diseases, cancers, metabolic syndromes, degenerative events, or trauma are linked to an elevated risk of adverse health outcomes and mortality (1-4). Myosteatosis involves ectopic infiltration of fat into skeletal muscle and has increasingly been recognized as a crucial component of muscular health. It exhibits a negative correlation with muscle mass, strength, and mobility representing a contributing factor to decreased muscle quality. While myosteatosis serves as an additional biomarker for sarcopenia, cachexia, and metabolic syndromes, it is not synonymous with sarcopenia, which specifically denotes the loss of muscle mass and function. Myosteatosis induces proinflammatory changes that contribute to decreased muscle function, compromise mitochondrial function, and increase inflammatory response in muscles (5).

Therefore, there is a need to quantify myosteatosis in the clinical setting of these disorders. However, since this infiltration of fat into the skeletal muscle is associated with both intermuscular and intramuscular adipose tissue (5,6), each of which provides a slightly different measure of myosteatosis and may represent different risk factors of muscle and metabolic health. A variety of imaging methods are now available for characterizing muscle health in both clinical practice and research, including ultrasound (US), computed tomography (CT), magnetic resonance imaging (MRI) and

magnetic resonance spectroscopy (MRS). However, due to technical limitations and the lack of a standardized definition, consensus on the optimal method or methods for assessing muscle quality with current imaging modalities has not yet been established. This review article aims to provide better understanding of the pathophysiological mechanisms and roles of myosteatosis, as well as describing imaging tools focused on new imaging approaches to assess fat in muscle as potential biomarkers of myosteatosis, and the most common clinical conditions involved.

Pathophysiological mechanisms and consequences of myosteatosis

In skeletal muscle, lipids are either stored as adipocytes visibly located between muscle groups and muscle fibres and within the muscle fascicles, corresponding to intermuscular adipose tissue (IMAT), or as triglycerides stored in adipocytes not visibly located outside muscle fibres in the interstitium as extramyocellular lipids (EMCL), and as lipid droplets in the cytoplasm within muscle fibres, known as intramyocellular lipids (IMCL) (6,7). The regulation and energy balance of IMAT, EMCL, and IMCL are multifaceted and interconnected (8). Age and lifestyle factors, such as physical activity, diet, and overall energy balance, play pivotal roles in shaping the accumulation and utilization of these lipid depots within skeletal muscles. Additionally, sex steroid deficiency, leptin deficiency, and treatments, such as glucocorticoids, stimulate myosteatosis. It is generally considered that fat deposits generate lipotoxicity with metabolic and cardiovascular consequences (9). The cellular origins of fatty accumulation in muscle arise through several different pathways, and intermuscular and intramuscular fat provide

slightly different measures of myosteatosis, potentially representing different risk factors for metabolic and muscle health (7).

IMAT is genuine adipose tissue with at least three cellular origins (muscle satellite stem cells and fibro-adipogenic progenitor cells resident in muscle, and adipose-derived stem cells that migrate from other adipose depots into the muscle tissue bed). The presence of IMAT is strongly associated with insulin resistance, type 2 diabetes mellitus (T2DM), and ageing. Moreover, it can affect the local muscle metabolic environment (10). While it constitutes a small proportion of total body adipose and subcutaneous adipose tissue (SAT), the quantity of IMAT in the entire body can be comparable to the amount of abdominal visceral adipose tissue (VAT). Increased IMAT is also positively associated with other adipose depots that correlate with cardiometabolic risk, including VAT and liver lipid content (11,12). Both VAT and IMAT increase with age and body mass index (BMI), whereas SAT decreases with age and increases in obesity. IMAT also increases in conditions such as sarcopenia associated with ageing and diseases, as well as metabolic syndromes such as T2DM, and muscular diseases or trauma, independently of SAT, while it can decrease in cachexia. In all these situations, there is an associated decrease in muscle mass, muscle strength, and performance, which is independent of the cross-sectional muscular area (10,13). The amount of IMAT varies considerably between individuals and muscles (5,14). In addition to identifying disparities between sexes and races/ethnicities, the amount of muscle fat can vary depending on the muscle performance and strength of an individual. Differences within an individual depend on the degree of muscle recruitment for each activity and regional differences in muscle metabolism associated with their aerobic or anaerobic capacity, resulting in variations between muscle groups that also increase with age (14).

The increase in EMCL and IMCL is influenced by mitochondrial function. EMCL is believed to serve as a long-term storage of local energy and has implications for muscle metabolism and insulin sensitivity (15). Located outside muscle fibres, EMCL can also be found between and around skeletal muscles, being referred to as IMAT. EMCL and IMAT having been associated with dysglycaemia, including insulin sensitivity and glucose tolerance, and with reduced muscle function, although their effects seem to differ from those of IMCL (10,16). IMCL is directly implicated in mitochondrial function, serving as a rapidly available source of energy during muscle contraction and regeneration. Its turnover is considered a marker of muscle metabolic health, and it is a risk factor for insulin resistance (5,15,17). The accumulation of IMCL is not homogeneous across different muscles or fibre types. Differences in IMCL content stored in various muscle types in athletes at rest are associated with cellular adaptation to differences in the type of exercise training and/or muscle fibre composition. Muscles with more oxidative activity and a higher percentage of such fibres, such as the soleus muscle, have more IMCL than those with more glycolytic activity, like the vastus lateralis. Nonetheless, lipid accumulation may support a transition of fast-twitch glycolytic fibres to a more oxidative phenotype, leading to a decrease in muscle power (7). An increase in IMCL is not always synonymous with muscular dysfunction. The athlete paradox revealed that chronic exercise training increases the muscle triglyceride component of IMCL due to increased muscular requirements, but this effect is independent of exercise effects on IMAT (10). On the other hand, differences in the subcellular localization of IMCL and lipid composition, including lipotoxic species such as diacylglycerols, ceramides and saturated IMCL, could have distinctive adverse effects on the insulin sensitivity of muscles (7,15,18).

Imaging assessment of myosteatosis

CT

A method widely used for diagnosing sarcopenia is CT, primarily assessing muscle mass by opportunistic imaging (2) and it is also commonly used to indirectly assess myosteatosis (5,6,19). The primary obstacle to the widespread use of CT images is radiation exposure (20). In this context, the use of low-dose CT can help reduce issues related to human exposure and, thus, support a broader application of CT in diagnostics. CT is employed for assessing muscle quantity with the skeletal muscle index (SMI) [muscle cross-sectional area (CSA)/height^2] and myosteatosis assessment typically involves measuring macroscopic accumulations of IMAT and muscle density or muscle attenuation (MA) (6,19). The radiodensity of the human thigh muscle obtained by CT correlates well with muscle triglyceride content (21). Typical anatomical locations for skeletal muscle measurements using CT include the thigh, proximal femur, trunk at the level of L3, cervical vertebrae, and some studies have included the upper and lower limbs (2,6,22,23). Muscle characteristics between L3 and thigh landmarks have shown a strong

correlation (24), while cervical levels have shown less reliable results (25). CT acquisition and reconstruction parameters vary widely across studies (6). To reduce radiation exposure, only one CT slice or a small range of several centimeters of a muscle is most often scanned (4,6).

The representative MA value can be obtained by a geometrically defined region of interest (ROI), or a volume of interest (VOI) placed in the muscle under study, such as a circle for slice-based analysis or a sphere or cylinder for volume-based analysis. The CT value of pure skeletal muscle is typically about 50–60 Hounsfield units (HU). Additional infiltration of extracellular lipids or adipose tissue within the muscle will decrease the muscle density value below 50 HU, with normal variations depending on sex and age (6,26). MA can also be measured by muscle segmentation using semi-automatic or automatic thresholds. Thresholds values commonly used to evaluate MA and muscle area are between –29 to 150 HU (6,22). A more detailed characterization of adipose tissue infiltration and its spatial distribution can be obtained based on the histogram of the CT values of the segmented muscle (14,27,28).

To evaluate IMAT, a qualitative or semi-quantitative grading of muscle structures based on a washed-out and moth-eaten muscle appearance on CT images has traditionally been applied in muscular dystrophies or congenital myopathies. This grading can be performed using the Mercuri score system, skill-based visually or through automated grading methods (28,29), or using the Goutallier classification to assess muscle fatty degeneration in rotator cuff tears (30). Another approach involves quantitative measurement based on semi-automatic or automatic segmentation of muscles, using threshold values between –190 to –30 HU to evaluate IMAT and adipose tissue (6,22). However, IMAT only accounts for approximately 3.3% to 8% of the total muscle area, making it ineffective for assessing the entire trunk or thigh muscle, and the measurement of only this adipose tissue may lead to an underestimation of the differences in myosteatosis among individuals (21,31).

CT measurements can be influenced by variations in patient factors, CT protocols, and measurement methods (19,32). Contrast-enhanced CT has been used to evaluate muscle density in opportunistic CT imaging performed for other purposes. However, clinically relevant differences in skeletal muscle density have been observed compared to non-contrast images and between contrast-enhancement phases. Additionally, significant intrasubject variations in contrast enhancement related to clinical status appear

to limit the simple correction of contrast-enhanced MA, even with a highly standardized injection and CT protocol (33-35). Nevertheless, measuring muscle fat using dual-energy CT in virtual non-contrast-enhanced images offers a promising new approach that allows assessment of muscle fat in contrast-enhanced opportunistic CT imaging (36).

Assessment of MA requires a calibration step, and the use of a calibration phantom should be considered (6,28). Other authors have proposed to normalize MA with the value of attenuation of the subcutaneous fat individually to avoid differences by the CT scanning conditions (37). Using CT thresholds of –29 to 150 HU for quantifying skeletal muscle and –190 to –30 HU for evaluating SAT, the sex-specific cutoff values for defining myosteatosis were MA >–0.44 in males and >–0.37 in females (38). The cutoff points for myosteatosis have mainly been studied in oncology, with most studies using the cutoff points of MA <41 HU for individuals with a BMI <25 kg/m^2 or MA <33 HU for those with a BMI ≥25 kg/m^2 (22,39). However, efforts are being made to develop useful indices for muscle quality measurements other than IMAT or MA to determine the diagnostic cutoff points for myosteatosis based on T-scores for use in various clinical situations. In this regard, the normal attenuation muscle area (NAMA) and the low attenuation muscle area (LAMA) and their indices have been analysed in trunk muscles (31,40), and the NAMA/total abdominal muscle area (TAMA) index has been proposed as an effective imaging biomarker for good-quality muscle for the assessment of myosteatosis (31). Additionally, since the NAMA/TAMA index is a ratio of two measurements made under the same condition, there is no impact on CT studies with contrast (41), making this an interesting alternative measure to muscle quality assessment in opportunistic contrast enhanced CT studies (*Figure 1*). Furthermore, the application of novel techniques enabling radiomic approaches for segmentation and quantification of the muscle-lipid distribution in CT images is being investigated using fully automated multiple-tissue three-dimensional (3D) segmentation or descriptors that quantify texture (4,27), opening new insights in feasibility and analysing larger body parts instead of single slices. The strengths and weaknesses of the CT measurements, as well as the proposed cutoff values for myosteatosis, are presented in *Tables 1,2*, respectively.

Quantitative magnetic resonance imaging (qMRI)

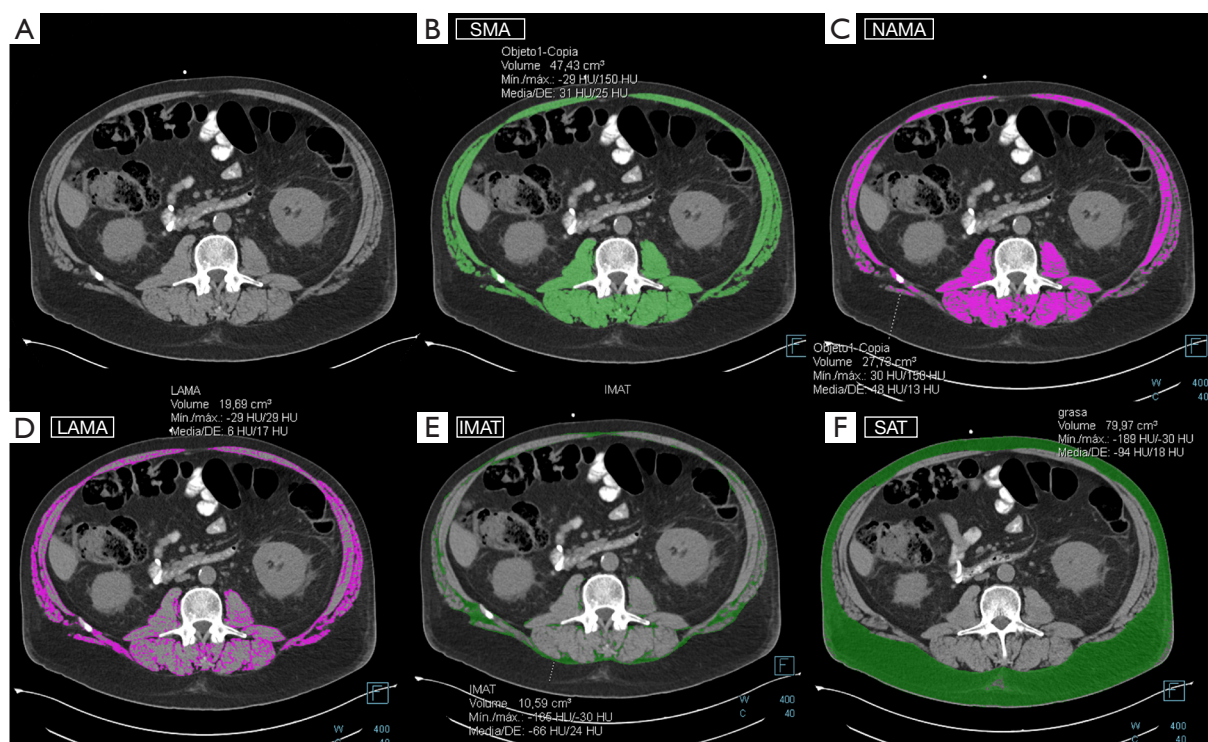MRI has superior soft tissue resolution and high contrast

Figure 1 Axial CT image at the level of L3 in a 66-year-old male patient with lung and gastrointestinal cancer and a BMI of 36.9 kg/m^2 (classified as obese with BMI >30 kg/m^2) (A). CT-based quantification with thresholds for MA of the (B) SMA, (C) NAMA, (D) LAMA, (E) IMAT, and (F) SAT were obtained using Syngo.via software (Siemens, Erlangen, Germany). CT-based parameters indicate myosteatosis. The MA was 31 HU (myosteatosis criteria for males is <33 HU for BMI ≥25.0 kg/m^2). The NAMA/TAMA index was 47% [myosteatosis criteria for males is <66.4% (T-score <2.0)]. The SAT was –94 HU and the MA/SAT index was –0.32 HU (myosteatosis criteria for males is >–0.44 HU). CT, computed tomography; BMI, body mass index; MA, muscle attenuation; SMA, skeletal muscle area; NAMA, normal attenuation muscle area; LAMA, low attenuation muscle area; IMAT, intermuscular adipose tissue; SAT, subcutaneous tissue attenuation; TAMA, total abdominal muscle area.

in the qualitative assessment of adipose tissue and muscle, resulting in better qualitative assessment compared to CT imaging, although MRI has lower spatial resolution than CT because it is affected by technical variations. MRI with standard spin-echo T1- and T2-weighted sequences allows qualitative and semiquantitative assessment of perceivable intermuscular fat or IMAT. Initially, for the semi-quantitative evaluation of muscular fat, CT semi-quantitative scores (e.g., Mercuri score and Goutallier classification) have been applied on T1-weighted spin-echo images (28,30), and have been adopted in different regions of the body and clinical situations. Advanced quantitative segmentation algorithms can determine fat content and the percentage of a muscle area or volume with more reproducible results than semi-quantitative evaluation (42). Quantitative assessment is particularly relevant for

evaluating potential differences in muscle composition compared to a healthy control (*Figure 2*), or for detecting any changes in muscle following an intervention. Different methods to determine thresholds for separating muscle and fat pixels have been used (43) as illustrated in *Figure 2A,2B*. Whole-body T1-weighted MRI sequences are of interest in myopathies affecting a large variety of muscles throughout the body (44) (*Figure 3*). However, imaging analysis of standard spin-echo sequences can be affected by complex artifacts, such as proton spin inhomogeneities.

qMRI to measure fat replacement of skeletal muscle, using either chemical shift imaging methods (Dixon or IDEAL), T1 and T2 mapping sequences, or MRS, has been demonstrated to provide a sensitive and primary objective in multiple studies. The chemical shift between water and fat is utilized in Dixon imaging to separate fat and water,

Table 1 Quantitative muscle parameters of myosteatosis by imaging technique

Measurement biomarkers	Procedure	Analyse	Strengths	Weak points
CT				
MA (HU)/phantom[a]		ROI/VOI	Opportunistic CT imaging	Radiation exposure
MA (HU)/SAT index[a]		ROI/VOI		Variability (patients, protocols, measurement methods)
MA (HU) histogram[b]		ROI/VOI		
IMAT semiquantitative		Visual	[b], detailed characterization of fat infiltration and its spatial distribution	[a], need calibration phantom or internal fat reference
IMAT (cm² or cm³) (%)[c]		Threshold		[c], underestimation of the differences among individuals
NAMA (cm²)		Threshold	[d], high accuracy	[c], needs correction with other measurement
LAMA (cm²)		Threshold		
TAMA (cm²)		Threshold		
NAMA/TAMA index (%)[d]				
MRI				
IMAT semiquantitative	T1–T2WI[b]	Visual	High resolution and contrast	Spatial resolution
IMAT (cm² or cm³) (%)[a]	T1–T2WI[b]	Threshold	Whole-body exams	
Fat (FF) (%)	DIXON[c]	ROI/VOI	[c], repeatable, reproducible, and accurate	[a], needs correction with other measurement
Fat and water (ms)	T1–T2 mapping[d]	ROI/VOI	[d], possibility of fast slice and volume analysis, option in paediatric population	[b], artifacts (magnetic field is not constant)
Fat (FF) (%) and water (ms)	MR Fingerprinting	ROI/VOI	[e], simultaneous FF and water T1–T2 maps	[d], T2 mapping unable to distinguish between oedema/ inflammation and fat infiltration
MRS				
Spectral peaks		VOI	Reference to validate PDFF (DIXON)	Sample error due to ROI position variance
EMCL (mmol/kg or IU)		VOI	Absolute muscle water and lipid content	Specialized software and expertise
IMCL (mmol/kg or IU)		VOI	Separation of IMCL and EMCL	Complex post-processing
Unsaturation index	3T or 7T / LCOSY	VOI	High accuracy and reproducibility	
US				
IMAT semiquantitative	Echo intensity	Visual	Availability	Inaccurate values in deep muscles
IMAT quantitative	Grayscale histogram	ROI	Radiation-free	Variability between US devices and by tissue conditions
	Elastography[b]	ROI	Bedside tool	Evaluation of both fat infiltration and fibrosis
				[b], indirect measurement of fat

CT, computed tomography; MA, muscle attenuation; HU, Hounsfield unit; ROI, region of interest; VOI, volume of interest; SAT, subcutaneous fat; IMAT, intermuscular fat; NAMA, normal attenuation muscle area (healthy muscle); LAMA, low attenuation muscle area (muscle with intramuscular lipids pool); TAMA, total abdominal muscle area; MRI, magnetic resonance imaging; FF, fat fraction; PDFF, proton density fat fraction; MRS, magnetic resonance spectroscopy; EMCL, extramyocellular lipids; IMCL, intramyocellular lipids; LCOSY, L-Correlated SpectroscopY; IU, institutional units; US, ultrasound.

Table 2 Quantitative CT measurements and cutoff values proposed for myosteatosis assessment

CT measurements	Anatomic landmarks	Thresholds	Cutoff values		References
			Male	Female	
MA (HU)	Abdominal wall muscles	−29 to 150 HU (muscle)	<41 HU, BMI <25* kg/m²	<41 HU, BMI <25* kg/m²	(22,39)
			<33 HU, BMI ≥25* kg/m²	<33 HU, BMI ≥25* kg/m²	
			<29.3 HU	<22.0 HU	(26)
	Psoas muscles		<33.3 HU	<31.1 HU	(22)
MA/SAT index (HU)	Abdominal wall muscles	−29 to 150 HU (muscle)	>−0.44	>−0.37	(38)
		−190 to −30 HU (SAT)	–	–	
NAMA (cm²)	Abdominal wall muscles	+30 to +150 HU (muscle)	–	–	(31,41)
LAMA (cm²⁾	Abdominal wall muscles	−29 to +29 HU (muscle)	–	–	
SMA (NAMA + LAMA) (cm²)	Abdominal wall muscles	−29 to +150 HU (muscle)	40.2 HU (T-score <2.0)	39.9 HU (T-score <2.0)	
TAMA (cm²)	Abdominal wall muscles	−190 to +150 HU (muscle)	34.1 HU (T-score <2.0)	33.5 HU (T-score <2.0)	
NAMA/TAMA index (%)	Abdominal wall muscles		66.4 (T-score <2.0)	65.1 (T-score <2.0)	
			73% for class I myosteatosis (−2.0 < T-score <−1.0)		
			66% for class II myosteatosis (T-score <−2.0)		
IMAT (cm²)	Abdominal wall muscles	−190 to −30 HU (muscle)	15.74 (T-score <2.0)	10.80 (T-score <2.0)	
IMAT/TAMA index (%)	Abdominal wall muscles		8.35 (T-score <2.0)	8.94 (T-score <2.0)	

*, applied in oncology. CT, computed tomography; MA, muscle attenuation; HU, Hounsfield unit; BMI, body mass index; SAT, subcutaneous fat; NAMA, normal attenuation muscle area (healthy muscle); LAMA, low attenuation muscle area (muscle with intramuscular lipids pool); SMA, skeletal muscle area; TAMA, total abdominal muscle area; IMAT, intermuscular fat.

providing a quantitative map of the muscle fat fraction on a voxel basis once the muscle has been segmented (44,45). Additionally, Dixon imaging allows the assessment of both intermuscular and intramuscular fat (45). Multi-echo Dixon techniques and intensity inhomogeneity correction, are recommended to reduce the B0-magnetic field inhomogeneity, enabling accurate quantification of fat content (45,46). Furthermore, the proton density fat fraction (PDFF) provides the most suitable measure, reflecting the true concentration of muscular triglycerides in any location. It allows precise measurement of muscle volume and the degree of fat infiltration, and can even separate intermuscular from intramuscular fat and is highly repeatable and reproducible, with the results being interchangeable with CT-derived measurements of muscle density (43-48). The fat fraction [% fat fraction = Signal_fat/(Signal_water + Signal_Fat) × 100] offers the most accurate assessment of muscle composition (43). Quantitative muscle measurements with fat fraction require previous segmentation. Advanced semi-automatic procedures, including deep learning-based fascia segmentation, as well as automated segmentation of individual muscles using various strategies, have been reported with accurate results (44,49) (*Figure 4*). These approaches are particularly crucial when conducting 3D analysis.

The T1 mapping sequence has demonstrated that T1 values can serve as a biomarker of fatty infiltrations and correlate with the fat-fraction measured by the three-point
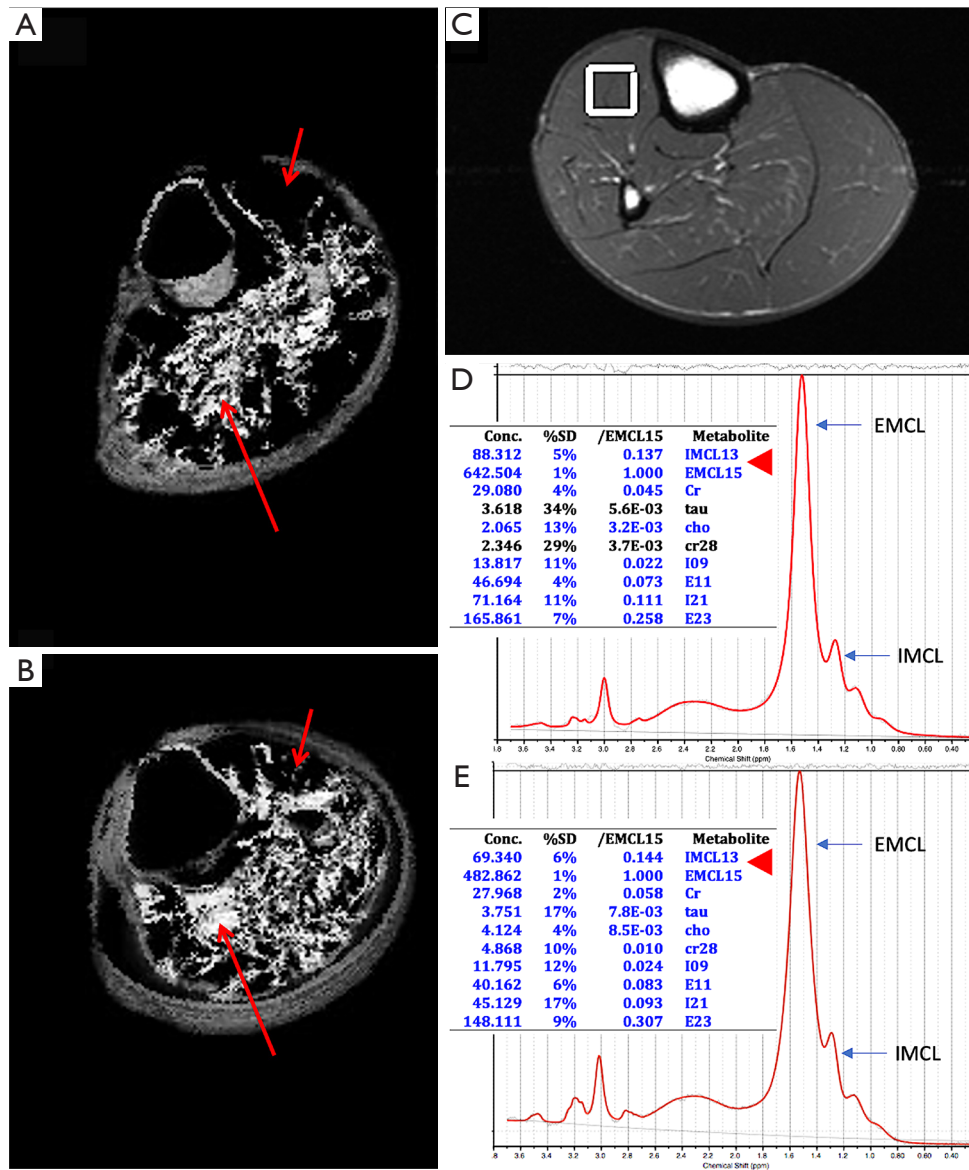
Figure 2 MRI-based quantification on T1-weighted images of the calf in a male patient with HIV-lipodystrophy and metabolic syndrome (A) and a healthy control (B), using Analyze 10.0 software with thresholds for IMAT (red long arrows) and MV (red short arrows). The patient (A) exhibited lower IMAT and higher MV than the healthy control (B). Localized 1-dimensional 1H-MRS using point-resolve spectroscopy data were collected from a voxel within the tibialis anterior muscle on axial T1-weighted image (C). LCModel software was employed to obtain spectra results, revealing that the patient (D) had higher IMCL and EMCL than the healthy control (E) (red arrowheads). EMCL, extramyocellular lipids; IMCL, intramyocellular lipids; SD, standard deviation; MRI, magnetic resonance imaging; IMAT, intermuscular adipose tissue; MV, muscular volume; 1H-MRS, proton magnetic resonance spectroscopy.

Dixon method (50,51). The T1-value decreases as the grade of fat infiltration increases and shows great potential for monitoring chronic muscular fatty infiltration (51). Fast T1 mapping, based on fast gradient echo trains and a flip angle <10°, provides high spatial resolution, allowing exploration of a wide range of areas. Due to its short acquisition time, it is a good candidate in cases in which rapid imaging is mandatory, such as in paediatric populations (50). T2 mapping has also been proposed as an imaging marker for fatty changes in skeletal muscle tissue because it allows the assessment of
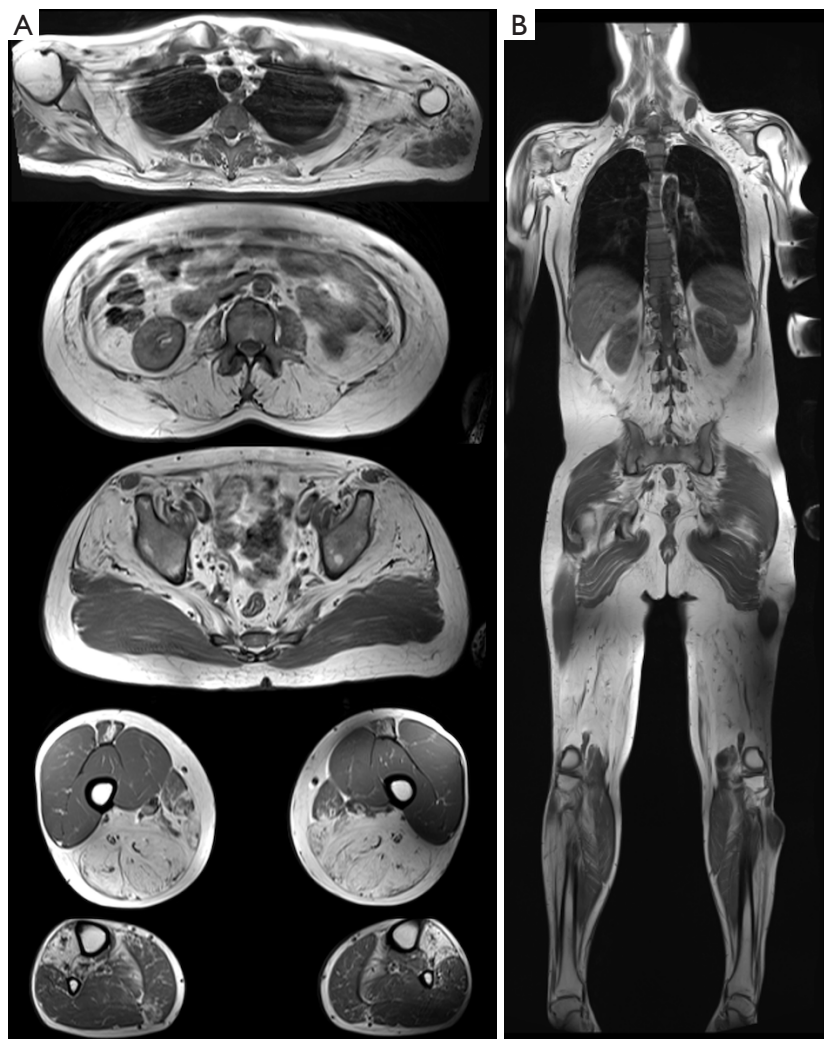
Figure 3 Whole-body muscle MRI in a patient with congenital muscular dystrophy (GNE or Nonaka myopathy). Axial (A) and coronal (B) T1-weighted images of various regions reveal a nearly symmetrical bilateral pattern of muscle fatty infiltration grades 3 (30–60%) and 4 (>60%), as assessed by the 5-point modified Mercuri scale, in several muscles of the different levels. MRI, magnetic resonance imaging.

small changes in muscle fibre composition. Measurements of T2 relaxation times can be used to identify an increase in T2 values due to microstructural changes in muscles infiltrated by fat (52). However, T2 mapping is unable to distinguish between oedema/inflammatory processes and fat infiltration, both of which result in an elevated T2-value. In contrast, T1 mapping is useful for this differentiation, since an oedema/inflammation process increases the T1-value, while fat infiltration decreases the T1-value (51). Recently, the magnetic resonance fingerprinting approach has been proposed for simultaneous quantification of T1, T2 and proton density, with a short acquisition time (53).

Proton magnetic resonance spectroscopy (^{1}H-MRS)

allows the determination of the fat fractions directly from the spectral peaks representing the lipids present, and it has become the reference to validate PDFF calculations (46). In clinical practice, Dixon imaging or T1 and T2 mapping has the advantage over spectroscopy because it can assess large and adjustable VOIs across volumetric data. In contrast, spectroscopy can determine fat content in a specific VOI, which may be associated with sample error due to variance in the VOI position (47,54). ^{1}H-MRS is the only imaging method that allows the separation of intracellular and extracellular lipids. It can determine absolute muscle water and lipid content with high accuracy and reproducibility not only using external referencing methods (expressed in
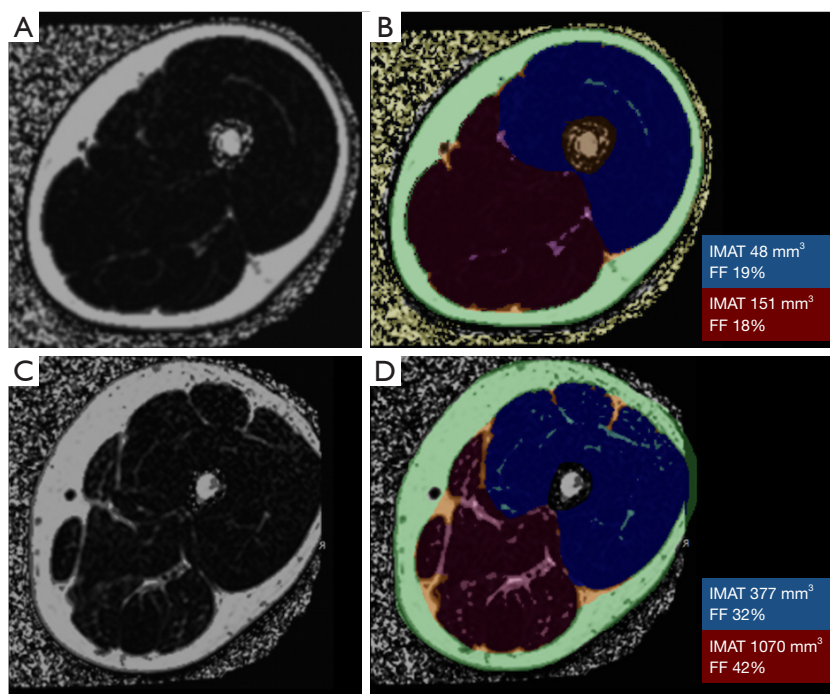
Quant Imaging Med Surg 2024;14(11):7937-7957 | https://dx.doi.org/10.21037/qims-24-365

Figure 4 Axial Dixon FF images of a healthy 26-year-old male with a BMI of 23 kg/m^2 (within the healthy weight range of BMI 18.5 to <25 kg/m^2), showing non-segmented (A) and segmented (B) images; and a healthy 31-year-old male with a BMI of 27 kg/m^2 (within the overweight range of BMI 25.0 to <30 kg/m^2), displaying non-segmented (C) and segmented (D) images. The male with overweight (C,D) exhibited myosteatosis with higher values of IMAT and FF in both flexor (red) and extensor (blue) compartments compared to the healthy weight male (A,B). FF, fat fraction; BMI, body mass index; IMAT, intermuscular adipose tissue.

mmol/kg) but also using internal referencing methods such as muscle water or creatine [expressed in institutional units (IU)] (55,56). ^{1}H-MRS can specifically quantify IMCL and EMCL, as shown in *Figure 2C-2E*, although EMCL protons are distributed heterogeneously in the muscle and can introduce variability in quantification (57). Consensus recommendations on how to perform ^{1}H-MRS in skeletal muscle have recently been published (58). Over the last few years, many studies have focused on evaluating the quality of IMCL and EMCL by the analysis of the unsaturation index and subspecies of lipid components more linked to metabolic risk, as well as other muscular metabolites (59,60). With the introduction of higher magnetic field strengths (3T and 7T) and novel MRS approaches, such as the development of two-dimensional (2D) spectroscopy sequences like L-correlated spectroscopy (L-COSY) (55,61,62) that allow improved spectral resolution for detecting different lipid components (*Figure 5*), or the development of multi-voxel spectroscopic imaging techniques with 3D coverage of the muscle (63), more comprehensive analysis of the skeletal muscle tissue will be

possible. ^{1}H-MRS has been widely used to study muscle physiology, exercise, and metabolic processes, as well as conditions such as chronic back pain, rotator cuff tears and muscular dystrophy (59,64,65). However, it is mainly used in research settings because it requires specialized software and expertise for spectral analysis. The strengths and weaknesses of both MRI and MRS measurements are presented in *Table 1*.

Musculoskeletal ultrasound (MSUS)

MSUS allows the assessment of muscle health by simultaneously evaluating muscle size, fascicle length, pennation angle, intramuscular fat infiltration and fibrous tissue through the analysis of echo intensity (EI), as well as muscular strain and stretch with shear wave elastography (SWE). The EI of the quadriceps femoris is known to be negatively correlated with quadriceps strength (66), and a strong association with MRI-based muscular PDFF has been reported (47). Although the extent to which MSUS can be used to quantify myosteatosis remains unknown, especially
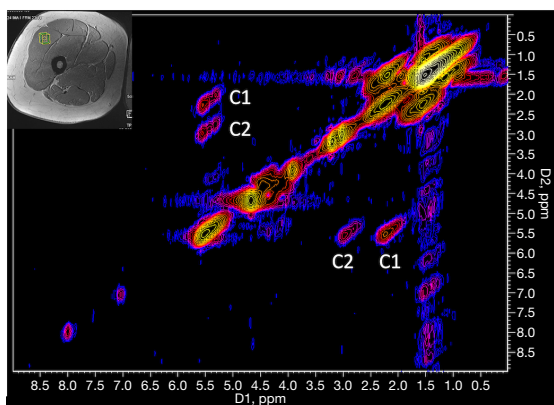
Figure 5 Localized 2D-COSY spectrum recorded of the vastus lateralis muscle (top left) in a healthy 46-year-old female subject. Post-processing was conducted using FELIX NMR software (Accelrys, San Diego, CA, USA), and a total of 22 peaks were measured. Monounsaturated lipid pools can be distinguished by the cross peaks C1 (5.3/2.1 and 2.1/5.3 ppm), and PUFAs by the cross peaks C2 (5.3–5.5/2.75–2.9 and 2.75–2.9/5.3–5.5 ppm). Ratios of these cross-peak volumes were used to define the degree of unsaturation. 2D-COSY, 2-dimensional correlation spectroscopy; NMR, nuclear magnetic resonance; PUFAs, polyunsaturated lipid pools.

in detecting variations due to ageing and disease (47), and no standardized protocol for the assessment of skeletal muscle has been established, particularly regarding which muscle group should be measured (67).

In the spectrum of sarcopenia and within the context of acute or chronic diseases, the muscles most commonly measured are the quadriceps muscle, specifically the rectus femoris and vastus intermedius, with the midpoint of the thigh serving as an anatomical landmark (68,69). Other muscle groups measured include the biceps brachii, tibialis anterior, flexor carpi radialis, and lumbar muscles (68). The Sarcopenia Ultrasound Group has attempted to provide a standardized technique for measuring muscle parameters by offering expert consensus guidelines (69), although recommendations regarding the most appropriate MSUS devices or settings are lacking. Bright mode (B-mode) US with a linear array probe (5–10 MHz) is commonly used in most studies (68,70), although 12 to 15 MHz probes have been applied with optimal results (71). The transverse view of the muscle improves the reliability of EI measurements, as well as the use of a larger ROI with a panoramic view (72,73). Other important recommendations for MSUS examinations include the generous use of contact gel, applying minimum pressure with the probe to avoid muscle

compression, and correctly placing the probe perpendicular to the area to be examined to prevent changes in muscle echogenicity related to anisotropy (71). Nevertheless, EI can also be affected by hydration, intra-/extracellular fluid balance, glycogen levels, and muscle damage. Additionally, because EI attenuates with depth, it can lead to inaccurate values in deep muscles (70). Several studies have reported stronger and less variable results when EI is corrected for the degree of subcutaneous adipose tissue thickness over the muscle (74). Taking subcutaneous fat thickness into consideration, MSUS imaging has been proposed for indirectly quantifying EMCL and IMAT based on EI (75).

The amount of fat in muscle tissue, along with measurements of fascicle length, pennation angle, and muscle stiffness, reflect the quality of skeletal muscle. Myosteatosis can be quantified by assessing the EI, which can be measured using a semiquantitative scale or through computer-aided grayscale analysis (71,76,77). In the past, a four-point visual grading scale for increased EI in muscles was proposed for muscular dystrophies, ranging from the visibility of bone echo to the complete disappearance of bone echo (78). More recently, a semiquantitative MSUS scoring system (71) was proposed, based on the severity of muscle degeneration on a three-point scale: Grade 1 defined as normal (preserved muscle architecture and echogenicity), Grade 2 defined as moderate changes (moderate/partial loss of muscle architecture and increased echogenicity), and Grade 3 defined as severe changes (severe or complete loss of muscle architecture and extensively increased echogenicity). This scoring system for sarcopenia has demonstrated high reliability and agreement, making the classification easier to apply (*Figure 6*).

Quantitative analysis of EI enables the detection of subtle changes in muscle composition. It can be achieved through computerized grayscale analysis using the grayscale histogram provided by several software programs and expressed in arbitrary units (ranging from 0 to 255, corresponding to black and white, respectively) of the largest possible ROI in the selected muscle during a transversal scan. A higher score indicates worse muscle quality (67,74) (*Figure 6*). It must be considered that EI measurements are more technically demanding and depend on US hardware and software, as well as the frequency, gain, tissue depth, and the analysis technique used (67,68). Higher variability has been observed between US devices for EI values >70, so it is recommended to use values with from the same US device and settings, especially when evaluating changes over time in patients with high muscle EI (67,79). The muscle ultrasonic image analysis
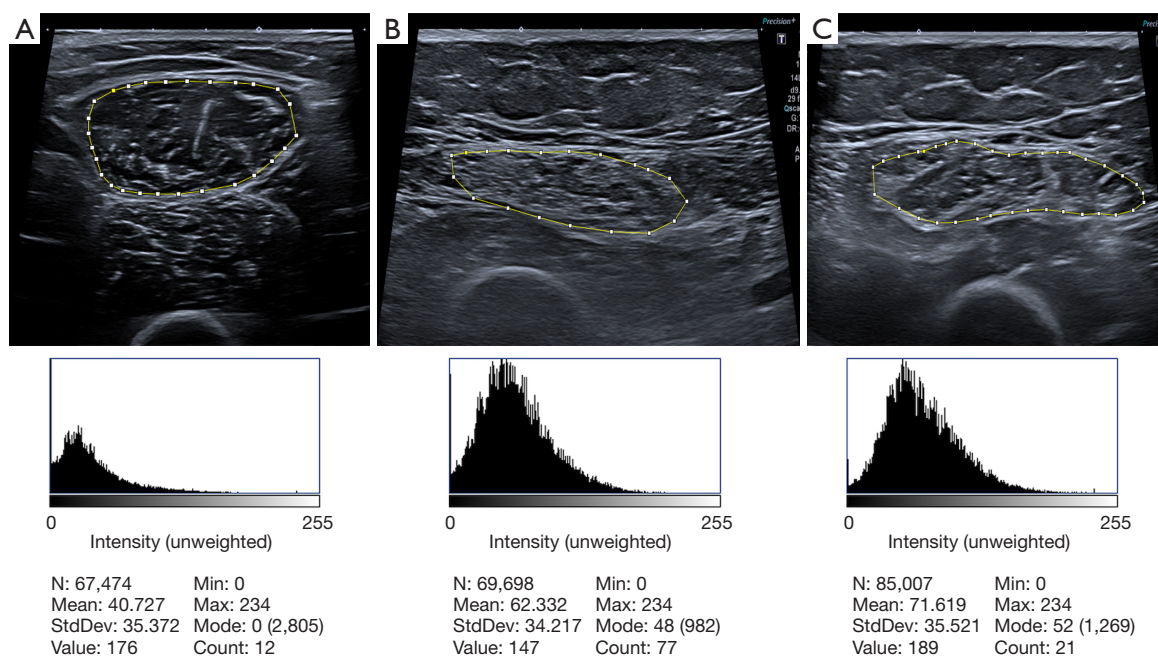
Figure 6 B-mode ultrasound transverse scan images of the rectus femoris muscle in a healthy 17-year-old female with preserved muscle architecture and echogenicity (A); a healthy 83-year-old female (B), and a healthy 68-year-old female (C), both exhibiting a moderate grade 2 of muscle degeneration (moderate/partial loss of muscle architecture and increased echogenicity). Muscle EI in grayscale and histographic analysis was performed using ImageJ software. The young healthy subject (A) demonstrated low EI. The middle-aged subject (C) with moderate muscle degeneration exhibited higher EI compared to the older subject (B). EI, echo intensity.

model developed based on artificial intelligence (AI) has shown advantages in various research studies. However, the application of AI in MSUS is currently limited to the analysis of grayscale US images, focusing on muscle segmentation, muscle structure analysis, and quantitative analysis of muscle EI (80). AI holds special potential for developing texture feature analysis in MSUS and its combination with other techniques such as elastography (80). Elastography has shown increased stiffness in patients with pathological changes related to muscle fat infiltration and fibrosis (47,81,82). Moreover, further research is required to correlate US EI with established reference techniques, such as CT or MRI, and to determine the time points at which myosteatosis changes occur and become pathological (47,68). The strengths and weaknesses of the MSUS measurements are presented in *Table 1*.

Clinical implications

Sarcopenia

Sarcopenia is a prevalent chronic disorder that commonly affects older adults; however, it can also manifest in association with various chronic systemic diseases linked to physical inactivity or inadequate intake of energy or protein. It may have an acute onset lasting less than six months and can be present in individuals who are in midlife or even younger (1,2). Sarcopenia is defined by low levels of muscle strength as the primary indicator of probable sarcopenia, low muscle quantity and quality, and poor physical performance as an indicator of severity (2,83). Muscle quantity and quality are considered the most critical factor for identifying sarcopenia. The European Working Group on Sarcopenia in Older People (EWGSOP) recommends the use of dual-energy X-ray absorptiometry (DXA) as a tool to diagnose sarcopenia in clinical practice, evaluating muscle quantity through the measurement of the appendicular lean mass index (83,84). However, DXA has several limitations, including low accuracy in estimating truncal fat and muscle, susceptibility to the influence of body fluids, overestimation of thigh muscle mass in obese individuals, and the inability to estimate muscle quality in terms of fatty infiltration (85). Recently, the EWGSOP stated the

importance of measuring myosteatosis (2), as it serves as a predictor of overall survival rates and adverse outcomes in patients with various cancers and chronic diseases, and both post-surgery and following trauma (39). CT and MRI are considered the gold standard for noninvasively assessing muscle quantity and myosteatosis (86).

CT is increasingly used in research trials as a routine diagnostic tool for assessing muscle quantity [using the CT-based SMI: CSA at L3 vertebral level divided by patient height^2 (cm^2/m^2)] and quality (using MA and IMAT). Recently, opportunistic CT imaging, primarily abdominal CT imaging performed for other purposes, has been widely applied to evaluate or predict outcomes in cancer and chronic diseases, revealing a link between impaired muscle quality at the L3 level, in addition to other sarcopenia-related changes and increased morbidity and mortality (19) (*Figure 1*).

MRI is a reliable method for evaluating muscle mass, and whole-body MRI is considered a gold standard technique for assessing muscle quantity. However, CSA measurements on a single slice in the axial plane, particularly at the mid-thigh muscles and lumbar vertebral level, are more frequently used (87). MRI provides robust imaging biomarkers for assessing muscle quality in sarcopenia, utilizing T1- and T2-weighted imaging for qualitative evaluation of fat in muscle; PDFF (*Figure 4*), T1 and T2 mapping to quantify myosteatosis; ^{1}H-MRS to depict lipid and other metabolite changes occurring in the intracellular environment in sarcopenia; as well as diffusion tensor imaging (DTI) for assessing architectural changes (52,85,87). While all of these MRI sequences are available in most MRI scanners, there are some challenges that need to be resolved in relation to protocol standardization, post-processing time, and result interpretation before the full integration of MRI into all clinical settings (44,45,52,85).

Recently, US has gained an important role due to its availability, enabling the evaluation of muscle mass, and muscle fibrosis/fatty replacement using EI (*Figure 6*). It also assesses other muscular quality parameters such as biomechanical muscle changes and muscle elasticity.

However, there is no consensus on the optimal methods, muscles to evaluate, measurement sites, or standardized acquisition protocols for any of these imaging assessments in sarcopenia (88). Although some cutoff values have been proposed for CT image (*Table 2*), the heterogeneity of the population evaluated, as well as the setting in which sarcopenia is investigated, impacts the techniques that are systematically adopted (89).

Metabolic syndrome

In recent years, myosteatosis has received significant attention in the context of metabolic syndrome, supported by consistent evidence indicating its association with dysglycaemia, insulin resistance, T2DM, and inflammation. Additionally, it has been linked to dyslipidemia independently of general obesity, VAT, and other relevant risk factors (90). These findings suggest that myosteatosis could potentially serve as a predictive tool for assessing metabolic risk (41,90). Conversely, metabolic syndrome and obesity have demonstrated a correlation with sarcopenia, as myosteatosis is accompanied by a reduction in lean body mass (91,92). Whereas in sarcopenia there is low muscle mass, creating a space within the fibre, and this space is filled with fat, in metabolic syndrome and obesity, myosteatosis precedes the functional decline of muscle, affecting muscle contractility and strength, compromising mitochondrial function, and increasing inflammatory response in muscle (5,41).

Muscle lipid metabolism assessed by ^{1}H-MRS has been studied over several decades in calf and quadriceps muscles, providing valuable mechanistic insights into metabolic changes in health and disease in a non-invasive way *in vivo*. ^{1}H-MRS research has focused on quantifying IMCL and EMCL, their unsaturation index, and subspecies of lipid components more closely linked to insulin resistance and metabolic risk, as well as other muscular metabolites (58-60,65) (*Figures 2C-2E,5*). This technique has proven to be especially valuable in investigating responses to exercise, meal challenges, and pharmacologic intervention. However, MRS is primary suitable for research purpose due to its complex postprocessing (58).

CT has been widely employed as a research tool to investigate muscle fat depots in metabolic syndrome studies, assessing IMAT and MA, which include NAMA and LAMA, in abdominal, thigh, and calf muscles, as well as SAT and VAT (90). The NAMA/TAMA ratio, derived from abdominal muscles, has been suggested as a robust index for quantifying myosteatosis (41). SAT and VAT are important parameters in the metabolic syndrome, with VAT being associated with cardiovascular risk. Quantitative analysis of VAT with CT imaging is more accurate than DXA, which may either overestimate or underestimate VAT volumes in patients with obesity and healthy individuals, respectively (93). Furthermore, considering that CT imaging can be opportunistically obtained in clinical practice, it becomes a potential tool in the evaluation of

metabolic syndrome. However, it is essential to define the specific muscle or muscles to be evaluated, as previous studies indicate variations among muscles (14). Standardized CT protocols need to be established, along with widely accepted HU cutoff points.

The use of US in the study of myosteatosis in metabolic syndrome has been limited. One study assessed the grayscale pixel intensity of the deltoid muscle and humeral cortex to calculate a muscle/bone ratio by US, yielding sensitive and accurate results for the detection of T2DM (94).

Neuromuscular disorders

Most neuromuscular disorders may present with muscle inflammation, fatty infiltrations, hypertrophy, or atrophy. These are traditionally assessed using standard T1-weighted and short tau inversion recovery T2-weighted MR sequences, which can focus on specific regions of the body, such as the lower limbs, or encompass the entire body in whole-body MRI (95,96). Fat replacement serves as a biomarker of disease progression, commonly evaluated with the semi-quantitative modified five-point Mercuri scale on T1-weighted or T2-weigthed DIXON sequences (95) (*Figure 3*). qMRI has emerged as a valuable modality for longitudinal assessment and therapy monitoring of these processes, with PDFF commonly used to quantify chronic muscular fatty degeneration (46,97). The T2 mapping sequence has been proposed for monitoring fatty replacement in skeletal muscle but has limitations in the presence of simultaneous muscle water and fat infiltration, which are frequently observed in some myopathies. This is because they cannot separate water and fat protons in the global muscle signal (44,50). In contrast, quantitative T1 mapping, fast T1 mapping, and recently developed magnetic resonance fingerprinting-based sequences have emerged as more robust methods for water-fat separation in evaluating fatty infiltration as well as functional alterations in neuromuscular diseases (50,53). Accurate and reliable muscle group segmentation, crucial for quantitative assessments, is evolving with the development of deep-learning-based methods as alternatives to atlas-based and conventional image analyses (49).

Regional myosteatosis

In several long cohort studies, muscle density on CT imaging was found to be more strongly associated with acute hip fracture than muscle size or bone mineral density (98), and served as an independent predictor of the risk of a second hip fracture (99). Both hip muscle size and density were correlated with mortality in older hip fracture patients, independently of age and clinical risk scores (100). Low muscular density of pelvic and thigh muscles was significantly correlated with the health-related quality of life of patients with hip osteoarthritis (101). Poor psoas muscle quality with low density negatively impacted outcomes after total hip arthroplasty (102). Conversely, increased postoperative physical activity after total hip arthroplasty enhanced the reduction of fatty muscular infiltration (103). Considering the protective role of pelvic and trunk muscle quality against hip fracture and in the outcomes of hip arthroplasty, it would be reasonable to include the assessment of fatty infiltration in these muscles in the evaluation of hip events and postoperative outcomes.

Recent reviews have explored the link between imaging-based changes in spinal muscles and spinal disorders (104). Previous studies identified the association of paraspinal muscle fat infiltration with low back pain, intervertebral disc degeneration, facet joint osteoarthritis, and poor physical function. The patterns vary based on aetiology, time course, and individuals (104-106). MRI is the preferred modality over CT or US due to its ability to assess multiple spinal structures. Various MRI studies have utilized parameters extracted from conventional axial T1- or T2-weighted sequences to assess fatty degeneration, focusing on signal intensity analysis or semi-quantitative scoring using the Goutallier classification. Thresholding approaches for estimating paraspinal muscle fat infiltration using T1- and T2-weighted MRI have been compared with chemical shift encoding-based water-fat MRI, showing low bias and absolute error (107). However, a most robust characterization using PDFF on MRI enables the detection of subtle changes in muscle composition at the early stages of paraspinal muscle degeneration (108). It also allows quantification of the pattern of muscular fat infiltration based on texture analysis of PDFF maps, improving the prediction of paraspinal muscle strength (109), with potential treatment implications.

The quality of the rotator cuff muscles is a crucial factor in clinical decision-making. Full-thickness rotator cuff tears are linked to accelerated fat deposition, and myosteatosis serves as a predictive imaging biomarker for post-surgical outcomes after rotator cuff repair (110). MRI is the primary modality for assessing rotator cuff tear and fat infiltration, often utilizing the five-point semi-quantitative Goutallier classification. Grade 3 muscles

(50% fat infiltration) indicate a relative contraindication to rotator cuff repair surgery. However, this semi-quantitative classification has suboptimal reproducibility. Quantitative methods, such as segmentation on T1-weighted images and fat fraction measurement with Dixon MRI, have demonstrated strong reliability (42,111), providing a viable alternative to the Goutallier classification system. US is frequently used in conjunction with MRI to assess rotator cuff pathology and muscle fatty infiltration. A scoping review on the use of quantitative US-based imaging for evaluating rotator cuff pathology revealed that both conventional B-mode US and SWE imaging were comparable to MRI-based techniques for assessing fatty infiltration and rotator cuff characterization (112). This indicates great promise for the quantitative evaluation of rotator cuff myosteatosis.

Intervention for myosteatosis

It is uncertain which lifestyle or pharmacological interventions can significantly impact myosteatosis levels. Recent studies indicate that physical activity may have a central role in reducing myosteatosis or preventing its accumulation (41,90,103). In cases of generalized myosteatosis, the addition of exercise to caloric restriction has been shown to increase IMAT reduction compared to either diet or exercise alone (10). To reverse myosteatosis, future large, well-designed, multidisciplinary intervention studies are necessary to investigate the combination of diet, exercise, and pharmacological interventions.

Conclusions

There is a need to use muscle-based biomarkers instead of muscle mass-based biomarkers to assess muscle health and to broaden the study of myosteatosis as an independent risk factor. Various techniques, including CT-based MA and IMAT quantification, MRI-based PDFF and T1–T2 mapping, and MSUS-based EI and SWE, are accessible in clinical practice and can be used as adjunct biomarkers of myosteatosis to assess various debilitating muscle health conditions. Recent studies on AI may provide further insights into quantification and automated assessment, including MRS analysis. This could reduce the time-consuming process and enable the analysis of larger body parts, potentially allowing the classification of patients at risk. However, to enhance clinical applicability, it is necessary to use standardized tools and measurements, including new imaging approaches that are easy to use. It is important to identify the specific muscles that should be examined and measured, and to establish widely accepted cutoff points. This will improve clinical practice and aid in identifying individuals at risk of poor outcomes. Furthermore, to ensure consistent application across studies and populations, it is imperative to establish a standardized definition of myosteatosis. Additionally, managing individuals at risk requires essential multidisciplinary collaborations that investigate the combination of diet, exercise, and medications.

Footnote

Provenance and Peer Review: With the arrangement by the Guest Editors and the editorial office, this article has been reviewed by external peers.

Conflicts of Interest: All authors have completed the ICMJE uniform disclosure form (available at https://qims.amegroups.com/article/view/10.21037/qims-24-365/coif). The special issue "Advances in Diagnostic Musculoskeletal Imaging and Image-guided Therapy" was commissioned by the editorial office without any funding or sponsorship. X.T. served as the unpaid Guest Editor of the issue. The authors have no other conflicts of interest to declare.

Ethical Statement: The authors are accountable for all aspects of the work in ensuring that questions related to the accuracy or integrity of any part of the work are appropriately investigated and resolved.

Open Access Statement: This is an Open Access article distributed in accordance with the Creative Commons Attribution-NonCommercial-NoDerivs 4.0 International License (CC BY-NC-ND 4.0), which permits the non-commercial replication and distribution of the article with the strict proviso that no changes or edits are made and the original work is properly cited (including links to both the formal publication through the relevant DOI and the license). See: https://creativecommons.org/licenses/by-nc-nd/4.0/.

7952

Garcia-Diez et al. Myosteatosis: diagnostic value and imaging approaches

References

1. Cruz-Jentoft AJ, Sayer AA. Sarcopenia. Lancet 2019;393:2636-46.
2. Cruz-Jentoft AJ, Bahat G, Bauer J, Boirie Y, Bruyère O, Cederholm T, Cooper C, Landi F, Rolland Y, Sayer AA, Schneider SM, Sieber CC, Topinkova E, Vandewoude M, Visser M, Zamboni M; Writing Group for the European Working Group on Sarcopenia in Older People 2 (EWGSOP2), and the Extended Group for EWGSOP2. Sarcopenia: revised European consensus on definition and diagnosis. Age Ageing 2019;48:601.
3. Xia L, Zhao R, Wan Q, Wu Y, Zhou Y, Wang Y, Cui Y, Shen X, Wu X. Sarcopenia and adverse health-related outcomes: An umbrella review of meta-analyses of observational studies. Cancer Med 2020;9:7964-78.
4. Prado CM, Ford KL, Gonzalez MC, Murnane LC, Gillis C, Wischmeyer PE, Morrison CA, Lobo DN. Nascent to novel methods to evaluate malnutrition and frailty in the surgical patient. JPEN J Parenter Enteral Nutr 2023;47 Suppl 1:S54-68.
5. Correa-de-Araujo R, Addison O, Miljkovic I, Goodpaster BH, Bergman BC, Clark RV, Elena JW, Esser KA, Ferrucci L, Harris-Love MO, Kritchevsky SB, Lorbergs A, Shepherd JA, Shulman GI, Rosen CJ. Myosteatosis in the Context of Skeletal Muscle Function Deficit: An Interdisciplinary Workshop at the National Institute on Aging. Front Physiol 2020;11:963.
6. Engelke K, Museyko O, Wang L, Laredo JD. Quantitative analysis of skeletal muscle by computed tomography imaging-State of the art. J Orthop Translat 2018;15:91-103.
7. Hamrick MW, McGee-Lawrence ME, Frechette DM. Fatty Infiltration of Skeletal Muscle: Mechanisms and Comparisons with Bone Marrow Adiposity. Front Endocrinol (Lausanne) 2016;7:69.
8. Komolka K, Albrecht E, Wimmers K, Michal JJ, Maak S. Molecular heterogeneities of adipose depots - potential effects on adipose-muscle cross-talk in humans, mice and farm animals. J Genomics 2014;2:31-44.
9. Engin AB. What Is Lipotoxicity? Adv Exp Med Biol 2017;960:197-220.
10. Goodpaster BH, Bergman BC, Brennan AM, Sparks LM. Intermuscular adipose tissue in metabolic disease. Nat Rev Endocrinol 2023;19:285-98.
11. Goodpaster BH, He J, Watkins S, Kelley DE. Skeletal muscle lipid content and insulin resistance: evidence for a paradox in endurance-trained athletes. J Clin Endocrinol Metab 2001;86:5755-61.
12. Yim JE, Heshka S, Albu J, Heymsfield S, Kuznia P, Harris T, Gallagher D. Intermuscular adipose tissue rivals visceral adipose tissue in independent associations with cardiovascular risk. Int J Obes (Lond) 2007;31:1400-5.
13. Delmonico MJ, Harris TB, Visser M, Park SW, Conroy MB, Velasquez-Mieyer P, Boudreau R, Manini TM, Nevitt M, Newman AB, Goodpaster BH; Health, Aging, and Body. Longitudinal study of muscle strength, quality, and adipose tissue infiltration. Am J Clin Nutr 2009;90:1579-85.
14. Daguet E, Jolivet E, Bousson V, Boutron C, Dahmen N, Bergot C, Vicaut E, Laredo JD. Fat content of hip muscles: an anteroposterior gradient. J Bone Joint Surg Am 2011;93:1897-905.
15. Kahn D, Perreault L, Macias E, Zarini S, Newsom SA, Strauss A, Kerege A, Harrison K, Snell-Bergeon J, Bergman BC. Subcellular localisation and composition of intramuscular triacylglycerol influence insulin sensitivity in humans. Diabetologia 2021;64:168-80.
16. Goodpaster BH, Carlson CL, Visser M, Kelley DE, Scherzinger A, Harris TB, Stamm E, Newman AB. Attenuation of skeletal muscle and strength in the elderly: The Health ABC Study. J Appl Physiol (1985) 2001;90:2157-65.
17. Kiefer LS, Fabian J, Rospleszcz S, Lorbeer R, Machann J, Kraus MS, Roemer F, Rathmann W, Meisinger C, Heier M, Nikolaou K, Peters A, Storz C, Diallo TD, Schlett CL, Bamberg F. Distribution patterns of intramyocellular and extramyocellular fat by magnetic resonance imaging in subjects with diabetes, prediabetes and normoglycaemic controls. Diabetes Obes Metab 2021;23:1868-78.
18. Laurens C, Moro C. Intramyocellular fat storage in metabolic diseases. Horm Mol Biol Clin Investig 2016;26:43-52.
19. Boutin RD, Lenchik L. Value-Added Opportunistic CT: Insights Into Osteoporosis and Sarcopenia. AJR Am J Roentgenol 2020;215:582-94.
20. Stuursma A, Stroot IAS, Vermeulen KM, Slart RHJA, Greuter MJW, Mourits MJE, de Bock GH. Reliability, costs, and radiation dose of dual-energy X-ray absorptiometry in diagnosis of radiologic sarcopenia in surgically menopausal women. Insights Imaging 2024;15:104.
21. Goodpaster BH, Thaete FL, Kelley DE. Composition of skeletal muscle evaluated with computed tomography. Ann N Y Acad Sci 2000;904:18-24.
22. Amini B, Boyle SP, Boutin RD, Lenchik L. Approaches

to Assessment of Muscle Mass and Myosteatosis on Computed Tomography: A Systematic Review. J Gerontol A Biol Sci Med Sci 2019;74:1671-8.

23. Shen Y, Levolger S, Zaid Al-Kaylani AHA, Uyttenboogaart M, van Donkelaar CE, Van Dijk JMC, Viddeleer AR, Bokkers RPH. Skeletal muscle atrophy and myosteatosis are not related to long-term aneurysmal subarachnoid hemorrhage outcome. PLoS One 2022;17:e0264616.

24. de Medeiros GOC, de Sousa IM, Chaves GV, Gonzalez MC, Prado CM, Fayh APT. Comparative assessment of abdominal and thigh muscle characteristics using CT-derived images. Nutrition 2022;99-100:111654.

25. Van den Broeck J, Sealy MJ, Brussaard C, Kooijman J, Jager-Wittenaar H, Scafoglieri A. The correlation of muscle quantity and quality between all vertebra levels and level L3, measured with CT: An exploratory study. Front Nutr 2023;10:1148809.

26. van der Werf A, Langius JAE, de van der Schueren MAE, Nurmohamed SA, van der Pant KAMI, Blauwhoff-Buskermolen S, Wierdsma NJ. Percentiles for skeletal muscle index, area and radiation attenuation based on computed tomography imaging in a healthy Caucasian population. Eur J Clin Nutr 2018;72:288-96.

27. Mühlberg A, Museyko O, Laredo JD, Engelke K. A reproducible semi-automatic method to quantify the muscle-lipid distribution in clinical 3D CT images of the thigh. PLoS One 2017;12:e0175174.

28. Aubrey J, Esfandiari N, Baracos VE, Buteau FA, Frenette J, Putman CT, Mazurak VC. Measurement of skeletal muscle radiation attenuation and basis of its biological variation. Acta Physiol (Oxf) 2014;210:489-97.

29. Nakayama T, Ishiyama A, Murakami T, Kimura E, Kuru S. Automatic calculation of Mercuri grades from CT and MR muscle images. Brain Dev 2019;41:870-7.

30. Goutallier D, Postel JM, Gleyze P, Leguilloux P, Van Driessche S. Influence of cuff muscle fatty degeneration on anatomic and functional outcomes after simple suture of full-thickness tears. J Shoulder Elbow Surg 2003;12:550-4.

31. Kim HK, Kim KW, Kim EH, Lee MJ, Bae SJ, Ko Y, Park T, Shin Y, Kim YJ, Choe J. Age-related changes in muscle quality and development of diagnostic cutoff points for myosteatosis in lumbar skeletal muscles measured by CT scan. Clin Nutr 2021;40:4022-8.

32. Lortie J, Gage G, Rush B, Heymsfield SB, Szczykutowicz TP, Kuchnia AJ. The effect of computed tomography parameters on sarcopenia and myosteatosis assessment: a scoping review. J Cachexia Sarcopenia Muscle 2022;13:2807-19.

33. van Vugt JLA, Coebergh van den Braak RRJ, Schippers HJW, Veen KM, Levolger S, de Bruin RWF, Koek M, Niessen WJ, IJzermans JNM, Willemsen FEJA. Contrast-enhancement influences skeletal muscle density, but not skeletal muscle mass, measurements on computed tomography. Clin Nutr 2018;37:1707-14.

34. Paris MT, Furberg HF, Petruzella S, Akin O, Hötker AM, Mourtzakis M. Influence of Contrast Administration on Computed Tomography-Based Analysis of Visceral Adipose and Skeletal Muscle Tissue in Clear Cell Renal Cell Carcinoma. JPEN J Parenter Enteral Nutr 2018;42:1148-55.

35. Boutin RD, Kaptuch JM, Bateni CP, Chalfant JS, Yao L. Influence of IV Contrast Administration on CT Measures of Muscle and Bone Attenuation: Implications for Sarcopenia and Osteoporosis Evaluation. AJR Am J Roentgenol 2016;207:1046-54.

36. Molwitz I, Leiderer M, McDonough R, Fischer R, Ozga AK, Ozden C, Tahir E, Koehler D, Adam G, Yamamura J. Skeletal muscle fat quantification by dual-energy computed tomography in comparison with 3T MR imaging. Eur Radiol 2021;31:7529-39.

37. Smith ACJ, Tse JJ, Waungana TH, Bott KN, Kuczynski MT, Michalski AS, Boyd SK, Manske SL. Internal calibration for opportunistic computed tomography muscle density analysis. PLoS One 2022;17:e0273203.

38. Feng H, Wang X, Mao L, Yu Z, Cui B, Lin L, Hui Y, Zhao X, Xu X, Fan X, Wang B, Yu Q, Jiang K, Sun C. Relationship between sarcopenia/myosteatosis and frailty in hospitalized patients with cirrhosis: a sex-stratified analysis. Ther Adv Chronic Dis 2021;12:20406223211026996.

39. Aleixo GFP, Shachar SS, Nyrop KA, Muss HB, Malpica L, Williams GR. Myosteatosis and prognosis in cancer: Systematic review and meta-analysis. Crit Rev Oncol Hematol 2020;145:102839.

40. Cuff DJ, Meneilly GS, Martin A, Ignaszewski A, Tildesley HD, Frohlich JJ. Effective exercise modality to reduce insulin resistance in women with type 2 diabetes. Diabetes Care 2003;26:2977-82.

41. Kim HK, Kim CH. Quality Matters as Much as Quantity of Skeletal Muscle: Clinical Implications of Myosteatosis in Cardiometabolic Health. Endocrinol Metab (Seoul) 2021;36:1161-74.

42. Davis DL, Kesler T, Gilotra MN, Almardawi R, Hasan SA, Gullapalli RP, Zhuo J. Quantification of shoulder muscle intramuscular fatty infiltration on T1-weighted MRI: a viable alternative to the Goutallier classification

system. Skeletal Radiol 2019;48:535-41.

43. Ogawa M, Lester R, Akima H, Gorgey AS. Quantification of intermuscular and intramuscular adipose tissue using magnetic resonance imaging after neurodegenerative disorders. Neural Regen Res 2017;12:2100-5.

44. Engelke K, Chaudry O, Gast L, Eldib MA, Wang L, Laredo JD, Schett G, Nagel AM. Magnetic resonance imaging techniques for the quantitative analysis of skeletal muscle: State of the art. J Orthop Translat 2023;42:57-72.

45. Huber FA, Del Grande F, Rizzo S, Guglielmi G, Guggenberger R. MRI in the assessment of adipose tissues and muscle composition: how to use it. Quant Imaging Med Surg 2020;10:1636-49.

46. Burakiewicz J, Sinclair CDJ, Fischer D, Walter GA, Kan HE, Hollingsworth KG. Quantifying fat replacement of muscle by quantitative MRI in muscular dystrophy. J Neurol 2017;264:2053-67.

47. Lortie J, Rush B, Osterbauer K, Colgan TJ, Tamada D, Garlapati S, Campbell TC, Traynor A, Leal T, Patel V, Helgager JJ, Lee K, Reeder SB, Kuchnia AJ. Myosteatosis as a Shared Biomarker for Sarcopenia and Cachexia Using MRI and Ultrasound. Front Rehabil Sci 2022;3:896114.

48. Faron A, Sprinkart AM, Kuetting DLR, Feisst A, Isaak A, Endler C, Chang J, Nowak S, Block W, Thomas D, Attenberger U, Luetkens JA. Body composition analysis using CT and MRI: intra-individual intermodal comparison of muscle mass and myosteatosis. Sci Rep 2020;10:11765.

49. Ogier AC, Hostin MA, Bellemare ME, Bendahan D. Overview of MR Image Segmentation Strategies in Neuromuscular Disorders. Front Neurol 2021;12:625308.

50. Marty B, Coppa B, Carlier PG. Monitoring skeletal muscle chronic fatty degenerations with fast T1-mapping. Eur Radiol 2018;28:4662-8.

51. Peng F, Xu H, Song Y, Xu K, Li S, Cai X, Guo Y, Gong L. Utilization of T1-Mapping for the pelvic and thigh muscles in Duchenne Muscular Dystrophy: a quantitative biomarker for disease involvement and correlation with clinical assessments. BMC Musculoskelet Disord 2022;23:681.

52. Chianca V, Albano D, Messina C, Gitto S, Ruffo G, Guarino S, Del Grande F, Sconfienza LM. Sarcopenia: imaging assessment and clinical application. Abdom Radiol (NY) 2022;47:3205-16.

53. Marty B, Reyngoudt H, Boisserie JM, Le Louër J, C A Araujo E, Fromes Y, Carlier PG. Water-Fat Separation in MR Fingerprinting for Quantitative Monitoring of the Skeletal Muscle in Neuromuscular Disorders. Radiology

2021;300:652-60.

54. Fischer MA, Nanz D, Shimakawa A, Schirmer T, Guggenberger R, Chhabra A, Carrino JA, Andreisek G. Quantification of muscle fat in patients with low back pain: comparison of multi-echo MR imaging with single-voxel MR spectroscopy. Radiology 2013;266:555-63.

55. Velan SS, Durst C, Lemieux SK, Raylman RR, Sridhar R, Spencer RG, Hobbs GR, Thomas MA. Investigation of muscle lipid metabolism by localized one- and two-dimensional MRS techniques using a clinical 3T MRI/MRS scanner. J Magn Reson Imaging 2007;25:192-9.

56. Boesch C. Musculoskeletal spectroscopy. J Magn Reson Imaging 2007;25:321-38.

57. Torriani M, Thomas BJ, Halpern EF, Jensen ME, Rosenthal DI, Palmer WE. Intramyocellular lipid quantification: repeatability with 1H MR spectroscopy. Radiology 2005;236:609-14.

58. Krššák M, Lindeboom L, Schrauwen-Hinderling V, Szczepaniak LS, Derave W, Lundbom J, Befroy D, Schick F, Machann J, Kreis R, Boesch C. Proton magnetic resonance spectroscopy in skeletal muscle: Experts' consensus recommendations. NMR Biomed 2021;34:e4266.

59. Brugnara L, García AI, Murillo S, Ribalta J, Fernandez G, Marquez S, Rodriguez MA, Vinaixa M, Amigó N, Correig X, Kalko S, Pomes J, Novials A. Muscular carnosine is a marker for cardiorespiratory fitness and cardiometabolic risk factors in men with type 1 diabetes. Eur J Appl Physiol 2022;122:1429-40.

60. Velan SS, Said N, Durst C, Frisbee S, Frisbee J, Raylman RR, Thomas MA, Rajendran VM, Spencer RG, Alway SE. Distinct patterns of fat metabolism in skeletal muscle of normal-weight, overweight, and obese humans. Am J Physiol Regul Integr Comp Physiol 2008;295:R1060-5.

61. Ramadan S, Ratai EM, Wald LL, Mountford CE. In vivo 1D and 2D correlation MR spectroscopy of the soleus muscle at 7T. J Magn Reson 2010;204:91-8.

62. Ramadan S, Mountford CE. Adiabatic localized correlation spectroscopy (AL-COSY): application in muscle and brain. J Magn Reson Imaging 2011;33:1447-55.

63. Wilson NE, Burns BL, Iqbal Z, Thomas MA. Correlated spectroscopic imaging of calf muscle in three spatial dimensions using group sparse reconstruction of undersampled single and multichannel data. Magn Reson Med 2015;74:1199-208.

64. Deshmukh S, Subhawong T, Carrino JA, Fayad L. Role of MR spectroscopy in musculoskeletal imaging. Indian J Radiol Imaging 2014;24:210-6.

65. van de Weijer T, Schrauwen-Hinderling VB. Application of Magnetic Resonance Spectroscopy in metabolic research. Biochim Biophys Acta Mol Basis Dis 2019;1865:741-8.

66. Fukumoto Y, Ikezoe T, Yamada Y, Tsukagoshi R, Nakamura M, Mori N, Kimura M, Ichihashi N. Skeletal muscle quality assessed from echo intensity is associated with muscle strength of middle-aged and elderly persons. Eur J Appl Physiol 2012;112:1519-25.

67. Ponti F, De Cinque A, Fazio N, Napoli A, Guglielmi G, Bazzocchi A. Ultrasound imaging, a stethoscope for body composition assessment. Quant Imaging Med Surg 2020;10:1699-722.

68. Casey P, Alasmar M, McLaughlin J, Ang Y, McPhee J, Heire P, Sultan J. The current use of ultrasound to measure skeletal muscle and its ability to predict clinical outcomes: a systematic review. J Cachexia Sarcopenia Muscle 2022;13:2298-309.

69. Perkisas S, Bastijns S, Baudry S, Bauer J, Beaudart C, Beckwée D, et al. Application of ultrasound for muscle assessment in sarcopenia: 2020 SARCUS update. Eur Geriatr Med 2021;12:45-59.

70. Nagae M, Umegaki H, Yoshiko A, Fujita K. Muscle ultrasound and its application to point-of-care ultrasonography: a narrative review. Ann Med 2023;55:190-7.

71. Möller Parera I, Miguel M, Blasi J, Piccaso R, Hammer HB, Ortiz-Sagrista J, Zaottini F, Martinoli C, Terslev L. Ultrasound assessment of degenerative muscle sarcopenia: the University of Barcelona ultrasound scoring system for sarcopenia. RMD Open 2023;9:e002779.

72. Varanoske AN, Fukuda DH, Boone CH, Beyer KS, Stout JR, Hoffman JR. Scanning plane comparison of ultrasound-derived morphological characteristics of the vastus lateralis. Clin Anat 2017;30:533-42.

73. Scott JM, Martin DS, Ploutz-Snyder R, Matz T, Caine T, Downs M, Hackney K, Buxton R, Ryder JW, Ploutz-Snyder L. Panoramic ultrasound: a novel and valid tool for monitoring change in muscle mass. J Cachexia Sarcopenia Muscle 2017;8:475-81.

74. Stock MS, Thompson BJ. Echo intensity as an indicator of skeletal muscle quality: applications, methodology, and future directions. Eur J Appl Physiol 2021;121:369-80.

75. Piponnier E, Ishikawa M, Kunimasa Y, Sano K, Jagot K, Boisseau N, Kurihara T, Martin V. Quantification of Extramyocellular Lipids and Intramuscular Fat from Muscle Echo Intensity in Lower Limb Muscles: A Comparison of Four Ultrasound Devices against Magnetic Resonance Spectroscopy. Sensors (Basel) 2023;23:5282.

76. Watanabe Y, Yamada Y, Fukumoto Y, Ishihara T, Yokoyama K, Yoshida T, Miyake M, Yamagata E, Kimura M. Echo intensity obtained from ultrasonography images reflecting muscle strength in elderly men. Clin Interv Aging 2013;8:993-8.

77. Harris-Love MO, Monfaredi R, Ismail C, Blackman MR, Cleary K. Quantitative ultrasound: measurement considerations for the assessment of muscular dystrophy and sarcopenia. Front Aging Neurosci 2014;6:172.

78. Heckmatt JZ, Leeman S, Dubowitz V. Ultrasound imaging in the diagnosis of muscle disease. J Pediatr 1982;101:656-60.

79. Pillen S, van Dijk JP, Weijers G, Raijmann W, de Korte CL, Zwarts MJ. Quantitative gray-scale analysis in skeletal muscle ultrasound: a comparison study of two ultrasound devices. Muscle Nerve 2009;39:781-6.

80. Li T, Ji F, Zhao R, Liu H, Yang M. Advances in the Research of Ultrasound and Artificial Intelligence in Neuromuscular Disease. Advanced Ultrasound in Diagnosis and Therapy 2023;7:122-9.

81. Pichiecchio A, Alessandrino F, Bortolotto C, Cerica A, Rosti C, Raciti MV, Rossi M, Berardinelli A, Baranello G, Bastianello S, Calliada F. Muscle ultrasound elastography and MRI in preschool children with Duchenne muscular dystrophy. Neuromuscul Disord 2018;28:476-83.

82. Drakonaki EE, Allen GM, Wilson DJ. Ultrasound elastography for musculoskeletal applications. Br J Radiol 2012;85:1435-45.

83. Costanzo L, De Vincentis A, Di Iorio A, Bandinelli S, Ferrucci L, Antonelli Incalzi R, Pedone C. Impact of Low Muscle Mass and Low Muscle Strength According to EWGSOP2 and EWGSOP1 in Community-Dwelling Older People. J Gerontol A Biol Sci Med Sci 2020;75:1324-30.

84. Messina C, Maffi G, Vitale JA, Ulivieri FM, Guglielmi G, Sconfienza LM. Diagnostic imaging of osteoporosis and sarcopenia: a narrative review. Quant Imaging Med Surg 2018;8:86-99.

85. Tagliafico AS, Bignotti B, Torri L, Rossi F. Sarcopenia: how to measure, when and why. Radiol Med 2022;127:228-37.

86. Heymsfield SB, Gonzalez MC, Lu J, Jia G, Zheng J. Skeletal muscle mass and quality: evolution of modern measurement concepts in the context of sarcopenia. Proc Nutr Soc 2015;74:355-66.

87. Vasilevska Nikodinovska V, Ivanoski S. Sarcopenia, More Than Just Muscle Atrophy: Imaging Methods for

the Assessment of Muscle Quantity and Quality. Rofo 2023;195:777-89.

88. Giovannini S, Brau F, Forino R, Berti A, D'Ignazio F, Loreti C, Bellieni A, D'Angelo E, Di Caro F, Biscotti L, Coraci D, Fusco A, Padua L, Bernabei R. Sarcopenia: Diagnosis and Management, State of the Art and Contribution of Ultrasound. J Clin Med 2021;10:5552. .

89. Tosato M, Marzetti E, Cesari M, Savera G, Miller RR, Bernabei R, Landi F, Calvani R. Measurement of muscle mass in sarcopenia: from imaging to biochemical markers. Aging Clin Exp Res 2017;29:19-27.

90. Miljkovic I, Vella CA, Allison M. Computed Tomography-Derived Myosteatosis and Metabolic Disorders. Diabetes Metab J 2021;45:482-91.

91. Barazzoni R, Bischoff SC, Boirie Y, Busetto L, Cederholm T, Dicker D, Toplak H, Van Gossum A, Yumuk V, Vettor R. Sarcopenic obesity: Time to meet the challenge. Clin Nutr 2018;37:1787-93.

92. Zhang H, Lin S, Gao T, Zhong F, Cai J, Sun Y, Ma A. Association between Sarcopenia and Metabolic Syndrome in Middle-Aged and Older Non-Obese Adults: A Systematic Review and Meta-Analysis. Nutrients 2018;10:364.

93. Kalisz K, Navin PJ, Itani M, Agarwal AK, Venkatesh SK, Rajiah PS. Multimodality Imaging in Metabolic Syndrome: State-of-the-Art Review. Radiographics 2024;44:e230083.

94. Rosen KA, Thodge A, Tang A, Franz BM, Klochko CL, Soliman SB. The sonographic quantitative assessment of the deltoid muscle to detect type 2 diabetes mellitus: a potential noninvasive and sensitive screening method? BMC Endocr Disord 2022;22:193.

95. Diaz-Manera J, Pichiecchio A, Santini F, Filosto M. Editorial: Imaging of Neuromuscular Diseases. Front Neurol 2021;12:814579.

96. Pace M, Cannella R, Di Stefano V, Lupica A, Alonge P, Morici G, Brighina F, Brancato F, Midiri F, Galia M. Usefulness and Clinical Impact of Whole-Body MRI in Detecting Autoimmune Neuromuscular Disorders. Brain Sci 2023;13:1500.

97. Schlaeger S, Sollmann N, Zoffl A, Becherucci EA, Weidlich D, Kottmaier E, Riederer I, Greve T, Montagnese F, Deschauer M, Schoser B, Zimmer C, Karampinos DC, Kirschke JS, Baum T. Quantitative Muscle MRI in Patients with Neuromuscular Diseases-Association of Muscle Proton Density Fat Fraction with Semi-Quantitative Grading of Fatty Infiltration and Muscle Strength at the Thigh Region. Diagnostics (Basel) 2021;11:1056.

98. Wang L, Yin L, Zhao Y, Su Y, Sun W, Liu Y, Yang M,

Yu A, Blake GM, Cheng X, Wu X, Veldhuis A, Engelke K. Muscle density discriminates hip fracture better than computed tomography X-ray absorptiometry hip areal bone mineral density. J Cachexia Sarcopenia Muscle 2020;11:1799-812.

99. Wang L, Yin L, Yang M, Ge Y, Liu Y, Su Y, et al. Muscle density is an independent risk factor of second hip fracture: a prospective cohort study. J Cachexia Sarcopenia Muscle 2022;13:1927-37.

100. Wang L, Yang M, Ge Y, Liu Y, Su Y, Guo Z, Huang P, Geng J, Wang G, Blake GM, He B, Yin L, Cheng X, Wu X, Engelke K, Vlug AG. Muscle size and density are independently associated with death after hip fracture: A prospective cohort study. J Cachexia Sarcopenia Muscle 2023;14:1824-35.

101. Iwasa M, Takao M, Soufi M, Uemura K, Otake Y, Hamada H, Sato Y, Sugano N, Okada S. Artificial intelligence-based volumetric analysis of muscle atrophy and fatty degeneration in patients with hip osteoarthritis and its correlation with health-related quality of life. Int J Comput Assist Radiol Surg 2023;18:71-8.

102. Shinonaga A, Matsumoto H, Uekawa M, Kuramoto A, Mitani S, Hagino H. Relationship Between Preoperative Psoas Major Muscle Quality and Forgotten Joint Score-12 in Patients After Total Hip Arthroplasty. Arthroplast Today 2023;20:101118.

103. Kawano T, Nankaku M, Murao M, Yuri T, Kitamura G, Goto K, Kuroda Y, Kawai T, Okuzu Y, Ikeguchi R, Matsuda S. Association of physical activity with fatty infiltration of muscles after total hip arthroplasty. Skeletal Radiol 2024;53:967-74.

104. Hodges PW, Bailey JF, Fortin M, Battié MC. Paraspinal muscle imaging measurements for common spinal disorders: review and consensus-based recommendations from the ISSLS degenerative spinal phenotypes group. Eur Spine J 2021;30:3428-41.

105. Hicks GE, Simonsick EM, Harris TB, Newman AB, Weiner DK, Nevitt MA, Tylavsky FA. Cross-sectional associations between trunk muscle composition, back pain, and physical function in the health, aging and body composition study. J Gerontol A Biol Sci Med Sci 2005;60:882-7.

106. Kalichman L, Carmeli E, Been E. The Association between Imaging Parameters of the Paraspinal Muscles, Spinal Degeneration, and Low Back Pain. Biomed Res Int 2017;2017:2562957.

107. Ornowski J, Dziesinski L, Hess M, Krug R, Fortin M, Torres-Espin A, Majumdar S, Pedoia V, Bonnheim

NB, Bailey JF. Thresholding approaches for estimating paraspinal muscle fat infiltration using T1- and T2-weighted MRI: Comparative analysis using water-fat MRI. JOR Spine 2024;7:e1301.

108. Sollmann N, Bonnheim NB, Joseph GB, Chachad R, Zhou J, Akkaya Z, Pirmoazen AM, Bailey JF, Guo X, Lazar AA, Link TM, Fields AJ, Krug R. Paraspinal Muscle in Chronic Low Back Pain: Comparison Between Standard Parameters and Chemical Shift Encoding-Based Water-Fat MRI. J Magn Reson Imaging 2022;56:1600-8.

109. Dieckmeyer M, Inhuber S, Schlaeger S, Weidlich D, Mookiah MRK, Subburaj K, Burian E, Sollmann N, Kirschke JS, Karampinos DC, Baum T. Texture Features of Proton Density Fat Fraction Maps from Chemical Shift Encoding-Based MRI Predict Paraspinal Muscle Strength. Diagnostics (Basel) 2021;11:239.

110. Lansdown DA, Lee S, Sam C, Krug R, Feeley BT, Ma CB. A Prospective, Quantitative Evaluation of Fatty Infiltration Before and After Rotator Cuff Repair. Orthop J Sports Med 2017;5:2325967117718537.

111. Davis DL, Zhuo J, Almardawi R, Mulligan ME, Resnik CS, Abdullah SB, Khalifah HA, Henn RF III, Gilotra MN, Hasan SA, Gullapalli RP. Association of Patient Self-Reported Shoulder Scores to Quantitative and Semiquantitative MRI Measures of Rotator Cuff Intramuscular Fatty Infiltration: A Pilot Study. AJR Am J Roentgenol 2019;213:1307-14.

112. Nasr AJ, Pierson CJ, Tzen YT, Khazzam M, Jain NB, Lin YS. Emerging Role of Quantitative Ultrasound-Based Imaging Techniques for Characterizing Rotator Cuff Tears: A Scoping Review. Diagnostics (Basel) 2023;13:2011.